energy&fuels

Article

pubs.acs.org/EF

Nanoparticles for Inhibition of Asphaltenes Damage: Adsorption Study and Displacement Test on Porous Media

Camilo A. Franco,[†] Nashaat N. Nassar,[‡,§] Marco A. Ruiz,[†] Pedro Pereira-Almao,[‡] and Farid B. Cortés*[,†]

[†]Grupo de investigación en Yacimientos de Hidrocarburos, Facultad de Minas, Universidad Nacional de Colombia Sede Medellín, Calle 59A No 63-20 Medellín, Columbia

[‡]Department of Chemical and Petroleum Engineering, University of Calgary, 2500 University Drive NW, Calgary, Alberta, Canada

[§]Department of Chemical Engineering, An-Najah National University, P.O. Box 7, Nablus, Palestine

ABSTRACT: The deposition of asphaltenes is one of the most difficult problems to overcome in oil production and processing. The presence of asphaltenes in crude oil, and consequently, the adsorption and deposition of asphaltenes on the rock surfaces, affects the rock properties, such as porosity, permeability, and wettability. This study aims at analyzing the effect of the chemical nature of 12 types of nanoparticles on asphaltenes adsorption; hence, the delay or inhibition of deposition and precipitation of asphaltenes on porous media under flow conditions at reservoir pressure and temperature were investigated. The adsorption equilibrium of asphaltenes onto nanoparticles was effectively achieved within relatively short times (approximately 2 min), which indicates the promising nature of adsorbents for delaying the agglomeration and inhibiting the precipitation and deposition of asphaltenes. The adsorption equilibrium of asphaltenes for the nanoparticles was determined using a batch method in the range 150−2000 mg/L. The equilibrium adsorption data were fit to both the Langmuir and Freundlich models. Additionally, in this study, the transport of nanoparticles in a porous media at a typical reservoir pressure and temperature was investigated. As a result, the use of nanoparticles allowed the system to flow successfully, which demonstrated the inhibition of precipitation and deposition and the enhanced perdurability against asphaltene damage in the porous media.

1. INTRODUCTION

Bitumen or heavy oil contains appreciable amount of asphaltenes that makes its transportation and processing complex and challenging. Asphaltenes are defined as the fraction of oil, bitumen, or vacuum residue that is insoluble in low-molecular-weight paraffins, such as *n*-heptane or *n*-pentane, yet is soluble in light aromatic hydrocarbons such as toluene, pyridine or benzene.[1,2] The asphaltenes structure is formed by polyaromatic cores attached to aliphatic chains containing heteroatoms, such as nitrogen, oxygen and sulfur, in addition to metals, such as vanadium and nickel.[3,4] Asphaltenes contain polar and nonpolar groups (i.e., amphiphilic behavior) with a tendency to form colloidal aggregates and to adsorb onto rock surfaces. The stability of asphaltenes in crude oil depends on a variety of factors rather than solely upon the asphaltenes content.[5] It has been demonstrated that the high asphaltenes content in the oil is not necessarily associated with the high risk of asphaltenes precipitation and deposition; to the contrary, relatively light oils, with low asphaltenes content are more prone to undergo asphaltenes precipitation and deposition, especially in subsaturated oil reservoirs, which are at pressures above the bubble point.[5]

The adsorption of previously precipitated asphaltenes onto mineral surfaces can lead to damage formation in oil reservoirs by reducing the oil effective permeability.[6] If the polar group of the asphaltenes molecular structure is adsorbed onto the rock surface, the rock wettability can be altered from water-wetting to oil-wetting, which affects the final oil recovery properties.[7]

Several researchers have studied the adsorption of asphaltenes onto solid surfaces with a focus on understanding the process phenomenology.[8−20] Pernyeszi et al.[16] studied the effect of different types of materials, such as clay minerals and different cores taken at different well depths on asphaltenes adsorption. The authors found that asphaltenes adsorption isotherms followed Type I behavior, according to the IUPAC classifications. Gonzalez et al.[15] reported that asphaltenes adsorption isotherms onto mineral surfaces followed Langmuir-type behavior with a maximum adsorption capacity of 1−2 mg/m^2. Other investigations on the adsorption of asphaltenes onto adsorptive clays also concluded that the isotherms exhibited Type I behavior, which indicates the formation of a monolayer on the porous matrix surfaces.[16−20] However, several researchers have reported multilayer adsorption of asphaltenes.[21−23] Acevedo et al.[21] obtained adsorption rate constants and adsorption isotherms on silica surfaces for toluene solutions of Furrial asphaltenes. The authors reported a slow tendency for the behavior to transition from L-type to H-type adsorption isotherms measured at different times. They argued that their results were affected by both the formation of asphaltenes multilayers at the silica surface and the adsorption of aggregates (e.g., dimers, trimers, etc.) as well as single asphaltenes molecules. Marczewski and Szymula[24−26] argued that the adsorption measurements of asphaltenes on several minerals cannot be sufficiently described by a simple model, such as the Langmuir model. They criticized other researchers for concluding prematurely that the isotherms are Langmuir-type and suggested that their conclusions were based only on the general shape of the isotherms without deeper insight into

Received: January 15, 2013
Revised: April 22, 2013

   dx.doi.org/10.1021/ef4000825 | *Energy Fuels* XXXX, XXX, XXX−XXX

their course. According to the authors, adsorption isotherms contain initial lines of Freundlich character with slope coefficients or/and inflections characteristic of lateral interactions as well as multiple steps, which may be related to surface phase reorientation, multilayer formation, or hemimicelle formation. However, asphaltenes may, as with any other molecule, present Langmuir type adsorption on some solids and more complex adsorption paths on many others. The fact that many authors have found irrefutable Langmuir isotherms for some solids simply mean that adsorption is not only depending on the nature of the adsorbate but also on the adsorbent. Typically, the adsorbed/deposited asphaltenes onto reservoir rocks are removed by solvents, surfactants, and other mechanical treatments.[27,28] These techniques are expensive and temporary because asphaltenes can easily redeposit. However, nanoparticles have gained investigators' attention due to their particular properties and possible application in the oil industry.[29] The idea stems from the unique properties of nanoparticles, such as their exceptionally high surface area to volume ratios, and functionalizable surface areas, which are crucial for adsorption rate, capacity, and selectivity.[30] Also, nanoparticles are highly mobile in porous media because they are much smaller than the relevant pore spaces, leading to effective transport.[31] Recently, Nassar et al.[32−34] reported asphaltene adsorption onto different surfaces of metal oxide nanoparticles and showed that the adsorption of asphaltenes is strongly dependent on the type of nanoparticles. Nanoparticles can adsorb the asphaltenes from crude oil and subsequently get adsorb onto porous media surfaces, hence, delaying the asphaltenes precipitation behavior with changes in pressure, temperature, and composition and altering the surface wettability according to the wetting preference of the nanoparticles.[35−40]

Although asphaltenes adsorption has been studied extensively, little work has been performed on the effect of nanoparticles on the delay or inhibition of asphaltenes precipitation. Recently, Mohammadi et al.[27] have employed nanoparticles of TiO_2, SiO_2, and ZrO_2 to enhance the stability of asphaltenes nanoaggregates through formation of hydrogen bonds at acidic conditions. The authors demonstrated that TiO_2 nanofluids, in a strongly acidic condition, can act as a dispersant, enhancing the stability of the asphaltenes and leading to a higher precipitation onset point. However, the authors did not evaluate adsorption phenomenon or the behavior of the nanofluids on porous media under flow conditions, at a typical reservoir pressures and temperatures. In this study, the effect of chemical nature of different types of nanoparticles on the delay of agglomeration or deposition of asphaltenes is investigated. The study focuses on the asphaltenes adsorption behavior and the flow on porous media at reservoir conditions under different nanofluid applications. The asphaltenes were extracted by *n*-heptane from a Colombian heavy crude oil.

2. EXPERIMENTAL SECTION

2.1. Materials. *2.1.1. Asphaltenes.* The "HOCHA" crude oil is produced from a reservoir located in the south of Colombia. The produced crude oil has 19.2°API (with a specific gravity of 0.9071) and viscosity of 230 cSt at 310.9 K. This crude oil was used to evaluate the development of nanoparticles in porous media. Also, the crude oil was used as a source of asphaltenes. Asphaltenes were extracted from the crude oil by *n*-heptane.

2.1.2. Solvents and Salt Precursors. Ethanol (99%, Merk KGaG, Germany) was used for in-house nanoparticle preparation. *n*-Heptane (99%, Sigma-Aldrich, U.S.A.) was used for asphaltenes extraction from crude oil. Tetraethyortosilicate (TEOS, 99%, Merck Schuchardt OHG, Germany), $Ni(NO_3)_2$ (Merk KGaG, Germany), $Pd(NO_3)_2$ (Merk KGaG, Germany), HNO_3(65%, CARLO ERBA Reactifs-SDS, Italy), and distilled water were used for synthesis of nanoparticles. A commercial surfactant provided by Petroraza SAS, Colombia, was used to disperse alumina nanoparticles in an aqueous solution for the preparation of the nanofluid.

2.2. Methods. *2.2.1. Asphaltene Extraction Protocol.* Asphaltenes were precipitated from HOCHA crude oil following a standard procedure.[30] In brief, an excess amount of *n*-heptane was added to the crude oil in a volume ratio of 40:1. The mixture was then sonicated for 2 h at 298 K and further stirred at 300 rpm for 20 h. Black precipitates formed at the bottom. The precipitated asphaltenes were collected after decanting the supernatant. Then, asphaltenes were washed with fresh *n*-heptane at a ratio 1:4 (g/mL), centrifuged at 5000 rpm for 15 min, and left to rest for 24 h. The asphaltenes were separated from the final solution by filtration using an 8-μm Whatman filter paper. The cake was washed with *n*-heptane several times until the color of the asphaltenes became shiny black. Finally, the obtained asphaltenes were homogenized and fined using pestle and mortar and left to dry at 298 K in a vacuum oven for 12 h. The model solutions for the batch adsorption experiments were prepared by dissolving a desired amount of the obtained asphaltenes in toluene. All samples were prepared from a stock solution containing 3000 mg/L asphaltenes diluted to different concentrations by addition of toluene. The initial concentration of asphaltene solutions used in the adsorption experiments ranged from 150 to 1500 mg/L.

2.2.2. In-house Prepared Nanoparticles. Silica nanoparticles were synthesized in-house using the sol−gel method.[39] The gel was prepared from TEOS, ethanol, water, and HNO_3. The synthesis was carried out following a procedure described elsewhere.[41,42] The molar ratio of TEOS/H_2O ranged from 1:4 to 1:8. The reactants were continuously stirred for 24 h at room temperature, and then, the mixture was centrifuged at 4000 rpm for 5 min to recover the nanoparticles and left to stand overnight. The obtained nanoparticles were washed with ethanol. Obtaining the particle sizes at the nanoscale required controlling the basicity and/or the TEOS/water molar ratio. Accordingly, two different sizes and structures of nanosilica gels were synthesized. Commercial silica gel purchased from Sigma-Aldrich, U.S.A., was used for comparison.

Using the incipient wetness technique, synthesized silica nanoparticles were impregnated with aqueous solutions of nickel nitrate $Ni(NO_3)_2$ at different mass percentages (5 and 15 wt %) for 3 h and then further dried at 393 K for 6 h. The obtained solid was calcined at 723 K for 6 h.[43] The hybrid nanomaterials obtained in this study are called supported hygroscopic salts (SHS) and denoted by the initial letter of the support followed by the symbol of the cation of the resulting metal oxide after calcination in addition to the weight percentage of the aqueous solutions of nickel nitrate $Ni(NO_3)_2$ used for impregnation. For instance, SNi15 denotes a SHS synthesized by using nanosilica gel as support and contain 15 wt % $Ni(NO_3)_2$, which would produce, after calcination, a nanosilica with NiO nanoparticles on its surface.

The same experimental procedure was used to impregnate $Ni(NO_3)_2$ on Al (supported alumina, purchased from Petroraza SAS, Colombia). Then, the sample was further dried at 393 K for 6 h. The obtained solid was calcined at 723 K for 6 h.[43] In a similar manner, an aqueous solution of 0.05 wt % of $Pd(NO_3)_2$ and 5 wt % of $Ni(NO_3)_2$ was used for the synthesis of PdNi/Al nanoparticles on the alumina support with the incipient wetness technique.[40] It should be noted here that the Ni and Pd precursors are hygroscopic salts. These materials become oxides after calcination. Table 1 lists the specifications of particle size and surface area characteristics of the nanoparticles used in this study.

2.2.3. Surface Area and Particle Size Measurements. The surface areas (S_{BET}) of the prepared nanoparticles were estimated following the Brunauer−Emmett−Teller (BET) method.[44,45] This was achieved by performing nitrogen adsorption−desorption at 77 K, using an Autosorb-1 from Quantacrome. The samples were degassed at 413 K

dx.doi.org/10.1021/ef4000825 | Energy Fuels XXXX, XXX, XXX−XXX

Table 1. Estimated Values of Nanoparticles Diameter ($d_{p\text{-}s}$), Supported Nanoparticle Diameter (d_p) and Surface Area (S_{BET}) of the Selected Nanoparticles

material	$d_{p\text{-}s}$ ± 0.03 nm	d_p ± 0.03 nm	S_{BET} ± 0.01 m^2/g	source
slica gel (crystalline), S	90.0		40.00	synthesized
SNi5	90.0	15.0	36.00	synthesized
SNi15	90.0	15.0	23.50	synthesized
fumed silica gel, SI	7.0		119.10	Sigma-Aldrich
silica gel (amorphous), SII	12.9		28.20	synthesized
silica gel (commercial), S III	7.0		232.30	Sigma-Aldrich
alumina I (commercial)	35.0		123.20	Petroraza
AlNi5	35.0	16.0	69.90	synthesized
AlNi15	35.0	29.0	17.90	synthesized
alumina II	45.0		223.20	Sigma-Aldrich
zeolite	16.		70.10	synthesized
PdNi/Al	35.0		221.30	synthesized
washed rock	mesh 60/40		15.00	Guadalupe Reservoir
unwashed rock	mesh 60/40		15.00	Guadalupe Reservoir

under N_2 flow overnight before analysis. Surface areas were calculated using the BET equation. The size of the nanoparticles was determined using an XPert PRO MPD X-ray diffractometer (PANalytical, Almelo, Netherlands), with Cu Kα radiation operating at 60 kV and 40 mA with a $\theta/2\theta$ goniometer. The mean crystallite size of the particles (d_p, nanoparticle diameter; $d_{p\text{-}s}$, supported nanoparticle diameter) was obtained by applying the Scherrer equation to the main diffraction peak.

2.2.4. Equilibrium Adsorption Isotherms. Batch adsorption experiments were carried out in a set of 10 mL vials by mixing together 100 mg nanoparticles with a 10 mL of the prepared heavy oil solution containing a certain concentration of asphaltenes at 298 K. The contents in the vials were agitated at 200 rpm by placing them in a temperature incubator and allowed to equilibrate for 24 h, as it was adequate time to achieve equilibrium.[30,33] The mixture was then separated, by allowing the nanoparticles containing adsorbed asphaltenes to precipitate and decanting the supernatant. The residual concentration of asphaltenes in the supernatant was measured by UV−vis spectrophotometry using a Genesys 10S spectrophotometer at a wavelength of 410 nm. A calibration curve of UV−vis absorbance at 410 nm against the asphaltenes concentration was established, using standard model solutions with known concentrations. UV−vis spectra of asphaltenes in solution were selected on the basis of the absorption linearity range, that is, absorbance <2.0. For high concentrations of asphaltenes (>250 mg/L), the asphaltenes solutions were diluted with toluene to the desired absorbance value and the actual concentration was estimated by multiplying the concentration of the diluted with the dilution factor. The adsorbed amount of asphaltenes (mg of asphaltenes/m^2 surface area of nanoparticles) was determined by the mass balance in eq 1:

$$Q = \frac{C_0 - C_E}{A} V \quad (1)$$

where C_0 is the initial concentration of asphaltenes in the solution (mg/L), C_E is the equilibrium concentration of asphaltenes in the supernatant (mg/L), V is the solution volume (L), and A is the dry surface area of nanoparticles (m^2).

2.3. Adsorption Modeling. Adsorption isotherms of asphaltenes onto different nanoparticles were modeled using the Langmuir and Freundlich models.

2.3.1. Langmuir Model. The Langmuir model has been widely used to correlate experimental data on equilibrium adsorption.[45,46] This model assumes that the process occurs on a homogeneous surface by monolayer adsorption. It was originally derived from the kinetic data of adsorption and desorption, taking into account the fact that equilibrium is obtained when the rates of adsorption and desorption are equivalent. The Langmuir equation can be expressed as follows:

$$N_{ads} = N_{ads,max}\left(\frac{K_L C_E}{1 + K_L C_E}\right) \quad (2)$$

where N_{ads} is the amount of asphaltene adsorbed onto the nanoparticles (mg/m^2), C_E is the equilibrium concentration of asphaltenes in the solution(mg/L), K_L is the Langmuir equilibrium adsorption constant related to the affinity of binding sites (L/mg), and $N_{ads,max}$ is defined as the monolayer saturation capacity, representing the maximum amount of asphaltenes adsorbed per unit surface area of nanoparticles for complete monolayer coverage (mg/m^2).

2.3.2. The Freundlich Model. Freundlich proposed an empirical expression to represent the isothermal variation of the adsorption of a quantity of mass adsorbed by unit mass of solid adsorbent at equilibrium concentration:[47]

$$N_{ads} = K_L C_E^{1/n} \quad (3)$$

where K_F is the Freundlich constant related to the adsorption capacity ($(mg/m^2)(L/mg)^{1/n}$), and $1/n$ is the adsorption intensity factor (unitless).It should be noted here that the Langmuir and Freundlich constants were estimated from the slopes and intercepts of the linear forms of eqs 2 and 3.[44]

2.4. Fluid Injection Test. *2.4.1. Porous Media.* A porous bed was selected to study the transport behavior of the nanoparticles through the porous media. The selected model porous media was clean silica sand (Ottawa sand, U.S. Sieves 30−40 mesh). The sands were purchased from Minercol S.A., Colombia. The porous medial has an absolute permeability of 2.19 Darcy and porosity of 33%. Before use, the sand was washed with deionized water to remove any dust or surface impurities and then was placed in a vacuum oven at 333 K for 12 h to evaporate any remaining water. Then, approximately 150 g of the sand was transferred to a stainless steel column for packing. The column has an inside diameter of 8 cm and length of 3.81 cm. The absolute permeability of the porous media was measured by injecting water after sand packing. Water was injected inside the porous media at a defined rate (0.5 mL/min), and two pressure transducers were used to record the pressure values at the injection and production points. Accordingly, the porous media permeability was estimated following Darcy's law.

2.4.2. Preparation of Nanoparticle Suspension (Nanofluid). For the fluid injection test, nanoparticle suspension was prepared by exposing a certain amount of Petroraza alumina nanoparticles to an aqueous mixture of 1% commercial surfactant provided by Petroraza SAS. The mixture was magnetically stirred at 298 K for 6 h and then sonicated at the same temperature for 24 h, whereby nanoparticles remained stable in suspension. The size of alumina nanoparticles in the aqueous solution was about 90 nm, as measured by a VASCO Particle Size Analyzer from Cordouan Technologies, France.

2.4.3. Experimental Setup and Procedure. Figure 1 shows a schematic representation of the experimental setup. The setup consists mainly of a tank containing the nanofluid, a commercial pump (Cole-Parmer Instrument Co., Canada), a positive displacement pump (DB Robinson Group, Canada), fraction collectors, and a stainless steel column reactor. Nanofluid mixtures were injected into the porous media from the injection point by positive displacement pump. In this case the oil and water are pumped to the filter for retaining any solid suspended in the fluid. Contrary to the nanofluid, which does not pass through of the filter. All tests were carried out at a temperature of 323 K and pore pressure of 6.9 MPa (maintained at this value with the pressure multiplier). To maintain reservoir conditions, the overburden

dx.doi.org/10.1021/ef4000825 | Energy Fuels XXXX, XXX, XXX−XXX

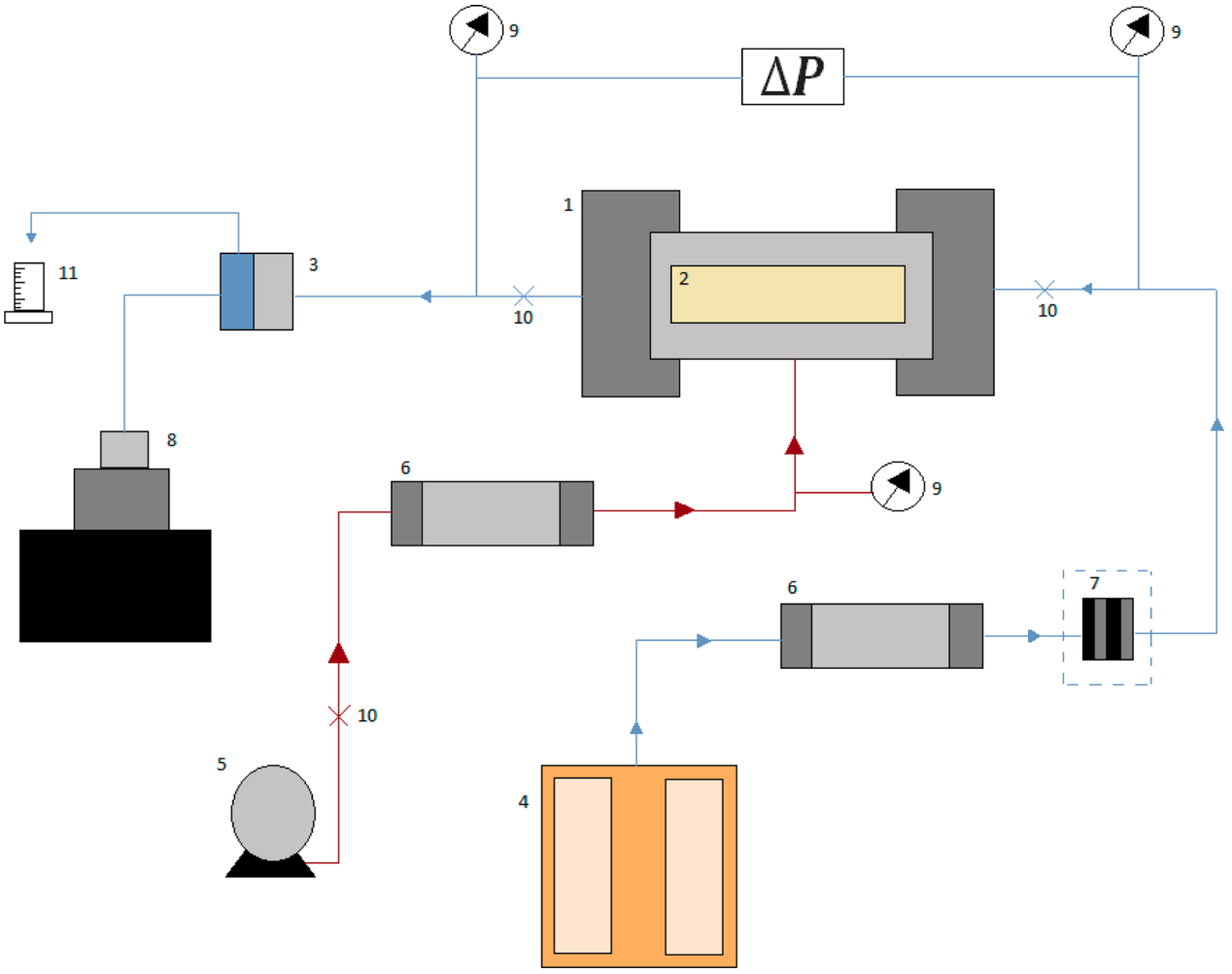

Figure 1. Diagram of the displacement test: (1) the core holder, (2) the core (Ottawa Sand Packing), (3) the pore pressure diaphragm, (4) pump one, the positive displacement pump, (5) pump two, (6) the displacement cylinder, (7) the filter, (8) the pressure multiplier, (9) the manometer, (10) a valve, and (11) the test tube.

pressure was kept at 6.9 MPa by pumping an incompressible fluid to the core holder with pump two, as indicated by the red flow line in Figure 1. To maintain test temperature, the outside body of the reactor column was covered with heating tapes and the column was insulated by fiber glass casing. A leak test was performed by pressurizing the packed bed reactor with pure nitrogen up to 6.9 MPa. A 1% change in pressure per hour was considered to be the maximum allowable pressure reduction during the leak test. Pressure was maintained at 6.9 MPa after the termination of the leak test. For the displacement tests on the porous media, the chemical nature of the nanoparticles and their concentration in the aqueous solution were selected on the basis of the isotherm results. The main objective of this displacement test was to evaluate the effectiveness of the nanoparticles for inhibiting the asphaltenes precipitation (e.g., formation of *i*-mers), the complex multimechanistic process (e.g., flocculation, precipitation, and layering) that causes rapid growth of deposits and subsequently reduces porosity and permeability of the flow channels and the deposition of asphaltenes. The displacement test was carried out by (1) constructing the base curves, (2) identifying the influence of the nanoparticles when asphaltenes damage (precipitation and deposition) was induced, and (3) finally, once the damage had been generated, observing the perdurability of the nanofluid treatment on the porous media.

For construction of the base curves, 10 pore volumes (PV) of water were injected to measure the absolute permeability at 323 K and 6.9 MPa (pore pressure). Then, at the same temperature, and under the saturation condition of residual water (Swr), the crude oil was injected until the pressure no longer changed. Finally, 20 PV of water were injected at 323 K to construct the relative permeability curves as functions of the water saturation. Accordingly, the recovery curves (Np) and the effective permeability to water at the saturation of oil residual (Sor) conditions were measured. For the evaluation of the effectiveness of nanoparticles after asphaltenes damage is induced, the packed bed was saturated with the injection of 2 PV of crude oil and the displaced volume of water in the porous media was measured. To study the inhibition or delay of asphaltenes precipitation, 0.5 PV of nanofluids was injected simultaneously with crude oil, followed by injection of 0.5 PV of *n*-heptane (a precipitation agent for asphaltenes) into the reactor. Immediately, the permeability with respect to the crude oil was measured. Then, 20 PV of water were injected to measure the relative permeability and Np curve. For induced asphaltenes damage, 50 PV of crude oil were injected to remove any chemical content in the porous media and the displaced water was measured. Then, 0.5 PV of *n*-heptane was injected to generate damage and measure the effective permeability with respect to oil. Finally, 20 PV of water were injected to measure the relative permeability for water and oil as well as the Np curve.

3. RESULTS AND DISCUSSION

3.1. Surface Characterization. Table 1 shows the BET surface area and particle size of the considered nanoparticles (commercially available and in-house prepared). Each type of nanoparticles exhibited a different chemical nature, size,

dx.doi.org/10.1021/ef4000825 | *Energy Fuels* XXXX, XXX, XXX–XXX

chemical structure, and surface area. Based on the X-ray measurement, the different silica nanoparticles prepared by the sol−gel method were structurally evaluated to be crystalline, fumed, and amorphous with the distinct sizes of 90, 7, 12.9 nm, respectively, and their BET surface area of 40, 119.1, and 28.2 m^2/g, respectively. As expected, for the hybrid materials, the surface area of the samples decreased as the content of NiO nanoparticles increased. This indicates that the deposition of NiO nanoparticles may block a portion of the pore space in the silica and alumina support.

3.2. Batch Adsorption Test: The Equilibrium Isotherm of Asphaltenes Adsorption on the Nanoparticles. Figure 2 shows the asphaltenes adsorption isotherms at 298 K for the

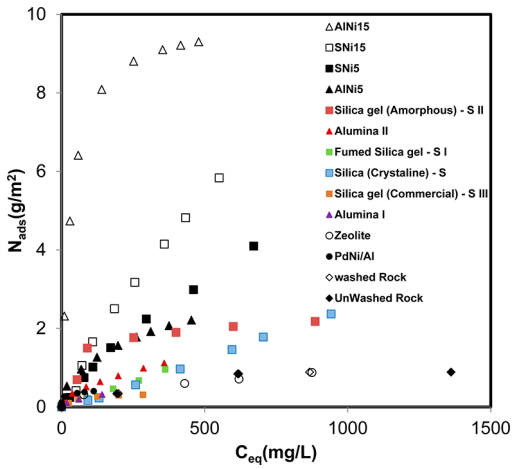

Figure 2. Experimental data for adsorption isotherms of asphaltenes onto different surfaces of nanoparticles at 298 K. Adsorbent dose, 10 g/L; shaking rate, 200 rpm.

selected nanoparticles. It should be noted here that the adsorption equilibrium of asphaltenes onto SHS could be reached within a relatively short time period (e.g., 2 min).[40] This finding shows potential industrial application for the nanoparticles as equilibrium time plays a major role in adsorption process as well as plant economic viability. As seen in Figure 2, all selected nanoparticles showed different adsorption affinity toward asphaltenes. This affinity was particularly demonstrated by the hybrid nanoparticles (i.e., the SHS samples). That is, the SHS samples adsorbed more asphaltenes than the support, regardless of the asphaltenes initial concentration, although this comparison was more noticeable at higher concentrations of asphaltenes (>300 mg/L). This observation can be attributed to the intermolecular forces (i.e., the polar interactions and electrical forces between the localized charges, which resulted from either permanent or induced dipoles) between the most polar components of the asphaltenes molecules (mainly the functional groups and heteroatoms) and the NiO supported on portions of the silica gel and alumina particle surfaces. Further, this high affinity toward asphaltenes also could be attributed to the significant dispersion of NiO on the surface of the hybrid nanomaterials. These results are in excellent agreement with those reported by Nassar et al.,[30] Cortés et al.,[39] Franco et al.[40] and Dudášová et al.,[48] who reported the asphaltene adsorption onto different surfaces of metal and metal oxide nanoparticles. It is worth noting that, in the concentration range in which the samples could be compared (0−750 mg/L), the asphaltenes uptake was higher for the SHS than the support. This was due to the fact that the presence of NiO nanoparticles on the support surface blocks a portion of the porosity in the alumina and silica gel supports, and consequently resulted in a reduction in the S_{BET} value for the SHS. However, the NiO also can adsorb asphaltenes, and in doing so, it compensates for the reduction in surface area and reduced asphaltenes uptake. That is, the adsorption of asphaltenes on the surface of the SHS was slightly higher than the asphaltenes uptake (mg/m^2) by the supports used, which was likely due to the low dispersion of NiO. Furthermore, at initial concentration of asphaltenes higher than 100 mg/L, the amount adsorbed of asphaltenes decreased in the order AlNi15 > SNi15 > SNi5 > AlNi5 ≈ SII > S > AlII > SI > Zeolite > PdNi/Al > AlI > washed rock ≈ unwashed rock > SIII. However, the asphaltenes adsorption at concentrations lower than 100 mg/L was higher in some nanoparticles; as a first approximation, this observation can be explained by Henry's constant. Henry's constant for asphaltenes adsorption depends weakly on the pore structure and geometry but strongly on the surface structure and chemistry of a given nanomaterial.[49] It is therefore highly important to analyze the uptake limit that can be achieved with adsorbents in which the adsorbing molecules on the surface are asphaltenes. However, if Henry's constants are within a suitable range to allow a significant degree of uptake, as with the typical homogeneous material, then modification of the pore structure toward a more homogeneous material may result in significantly improved uptake. This can be explained by an increase in the number of binding sites with high asphaltenes affinity, which mainly results from the increasing concentration of NiO in the SHS.

The surface chemistry and morphology of the nanoparticles as well as the chemical nature and physical properties of the asphaltenes define the nature of the asphaltenes—surface adsorption phenomenon. As shown in Table 1, the nanoparticles may differ in particle size, chemical structure, and surface chemistry. Such differences can affect the adsorption characteristics. It is interesting to note that, on a surface area basis, the alumina (AlI), the rocks, and the silica gel (SIII) did not show a significant affinity for asphaltenes adsorption. These results may be due to effects of the surface chemistry and functionality.

Figure 2 shows the asphaltenes adsorption onto the nanoparticles (both the support and the hybrids) at 298 K. The hybrid materials show a higher uptake than the support. The differences are due to the increased affinity of hybrid nanomaterials in comparison with the support and can be seen mainly in the Henry regions (at low concentrations). At 298 K, the highest adsorbing nanomaterial (SHS) was AlNi15, which adsorbed a maximum of 9 mg/m^2, while the silica gel (SIII) only adsorbed 0.5 mg/m^2. The nanomaterials with NiO impregnated on the support surface exhibited favorable uptake capacities. The crystal size of NiO depends on the concentration of impregnated salt; that is, at 5 and 15 wt % of NiO impregnation, the crystal sizes were 16 and 29 nm. Additionally, the results of the asphaltene adsorption show that alumina was the best support for the synthesized the SHS and not the silica gel (S).

3.3. Adsorption Model. The shapes of the isotherms were fit to the Langmuir and Freundlich models,[46,47] which are expressed in eqs 2 and 3, respectively. The adsorption equilibrium data for all selected nanoparticles fit very well to either Langmuir or Freundlich models, depending on the nanoparticle surface. This indicates that the selected nanoparticles have different surface structure and functionality.[50]

dx.doi.org/10.1021/ef4000825 | Energy Fuels XXXX, XXX, XXX−XXX

Table 2. Estimated Parameters for the Langmuir and Freundlich Models at 298 K

	Freundlich			Langmuir		
material	K_F ((mg/m^2)(L/mg)$^{1/n}$)	$1/n$	R^2	$N_{ads,max}$ (mg/m^2)	K_L (L/mg)	R^2
slica gel (crystalline), S	0.001	1.111	0.99	13.158	0.003	0.78
SNi5	0.027	0.769	0.99	8.961	0.001	0.85
SNi15	0.031	0.833	0.99	16.367	0.001	0.92
fumed silica gel, SI	0.235	1.047	0.99	NA	NA	NA
silica gel (amorphous), SII	0.362	0.271	0.95	2.189	0.040	0.98
silica gel (commercial), SIII	0.033	0.391	0.95	0.312	0.070	0.96
alumina I (commercial)	0.049	0.527	0.99	1.424	0.009	0.92
AlNi5	0.150	0.442	0.99	2.510	0.012	0.94
AlNi15	1.984	0.260	0.96	10.160	0.030	0.99
alumina II (commercial)	0.002	0.555	0.99	0.356	0.070	0.93
zeolite	0.042	0.445	0.99	0.892	0.084	0.97
PdNi/Al	0.178	0.171	0.99	0.411	1.222	1.00
washed rock	0.014	0.616	0.98	0.866	0.043	0.92
unwashed rock	0.053	0.398	0.93	0.889	0.043	0.96

Some have a homogeneous surface while others have a heterogeneous one. Langmuir and Freundlich fitted parameters are tabulated in Table 2. It can be observed that, for some of the nanoparticle surfaces, the $N_{ads,max}$ value differs widely for different nanoparticles. The same goes with the K_F values for the heterogeneous surfaces. In case of the materials with the better fitting to the Langmuir model in terms of R^2, and on surface area basis, a comparison of $N_{ads,max}$ values shows that the AlNi15 exhibits the highest adsorption capacity. $N_{ads,max}$ of the selected nanoparticles followed the order AlNi15 > SII >PdNi/Al > SIII. Figure 3 presents the theoretical Langmuir isotherms

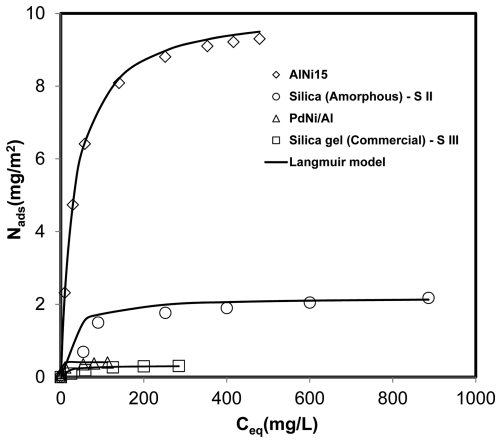

Figure 3. Correlation with the Langmuir model and experimental data of asphaltene onto AlNi15, silica amorphous, and PdNi/Al adsorption isotherms. The symbols are experimental data, and the solid lines are from the Langmuir model (eq 2).

against the experimental data for the materials that follow the Langmuir behavior. In this study, AlNi15 is one of the few that follows a Langmuir adsorption, which means is the one that does not tend to form multilayers adsorption but, above all, is surely the one that captures the most polar heavy compounds. Therefore, AlNi15 nanoparticles would inhibit asphaltenes layering which consequently cause permeability reduction.

The quality of adsorption measured by K_L values has the following order: PdNi/Al > S III > S II > AlNi15. SHS with 15 wt % NiO nanoparticles exhibits the highest values of $N_{ads,max}$. This could be due to the increase in number of binding sites with high asphaltenes affinity, which resulted from the increased concentration of NiO in the SHS sample. This is in excellent agreement with the result reported by Nassar et al.,[33] who showed that NiO nanoparticles has the highest adsorption affinity toward asphaltenes. The differences in adsorption affinity can be attributed to a different degree of interaction between nanoparticle homogeneous surface and asphaltenes.[33] It appears that SHS with high loading of NiO nanoparticles have better interaction with asphaltenes, as compared to other particles. These differences in ranking have been reported recently by Nassar et al.[33] on the adsorption of Athabasca C7-asphaltenes onto different surfaces of metal oxide nanoparticles. Nassar et al.[33]concluded that basic oxides, such as CaO and MgO, and amphoteric oxides, such as Fe_3O_4 and Co_3O_4, demonstrate higher adsorption capacity as compared to acidic oxides, such as TiO_2 and NiO. However, the quality of adsorption measured by adsorption affinity values (K_L) is higher for acidic oxides (with CaO being an exception). The authors suggested that strong interactions present between asphaltenes and nanoparticles are likely to increase the catalytic effect of nanoparticles with high K_L values for various reactions.

For the case of the materials with the better fitting to the Freundlich model in terms of R^2, the K_F values of the selected nanoparticles followed the order SI > AlNi5 > alumina I > zeolite > SNi15 > SNi5 > washed rock > alumina II > S, while the quality of adsorption measured by n values has the order S > SI > SNi15 > SNi5 > washed rock > Al II >Al I > zeolite > AlNi5. This suggests that asphaltenes were adsorbed onto a heterogeneous surface by multisites or multilayers adsorption having different adsorption energy; this was particularly true for the SHS nanoparticles. Once again, these differences show that the selected nanoparticles have different interaction behavior toward asphaltenes. This is in good agreement with study reported by Nassar et al.[51] on the adsorption and oxidation of asphaltenes onto alumina with varying surface acidity (i.e., acidic, basic, and neutral).[51] The authors reported different adsorption behavior asphaltenes onto acidic, basic, and neutral surface of alumina, and the adsorption capacities of asphaltenes onto the three aluminas followed the order acidic > basic and neutral.

3.4. Displacement Test. Following the batch adsorption test results, alumina I nanoparticles were used for preparing an aqueous nanofluid. Accordingly, for the displacement test, an aqueous solution containing 500 mg/L alumina nanoparticles was prepared at a high pressure and temperature (the reservoir

dx.doi.org/10.1021/ef4000825 | Energy Fuels XXXX, XXX, XXX−XXX

condition). The aim of this investigation was to see whether the nanoparticles were able to avoid agglomeration and inhibit the formation of damage, which is caused by the precipitation and subsequent deposition of asphaltenes. Table 3 displays the

Table 3. Estimated Values for Oil Effective Permeability, Water Effective Permeability, Saturation of Water Residual, and Saturation of Oil Residual at Different Periods: Before the Nanoparticle Injection (BN); after the Nanoparticle Injection (AN); and after the Induced Damage (AD)

	period		
property	BN	AN	AD
oil effective permeability (mD)	521.51 ± 0.01	696.24 ± 0.01	389.92 ± 0.01
water effective permeability (mD)	473.10 ± 0.01	329.39 ± 0.01	215.33 ± 0.01
saturation of oil residual (%)	25	21	30
saturation of water residual (%)	7	23	5

results obtained from the displacement test. In terms of permeability, clearly the nanoparticles cause an increase in the oil effective permeability (Ko) from 521 to 696 mD at the maximum oil saturation. Further, the nanoparticles induce a decrease in water effective permeability (Kw) from 473 to 329 mD at the maximum water saturation, which indicates an improvement in the mobility of oil and a reduction of 47% in the mobility of water.

Figure 4 shows the relative permeability curves for each of the three steps in the displacement test. Within the wide range

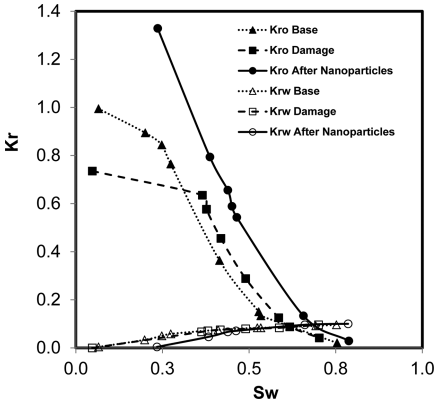

Figure 4. Relative permeability curves for the base system, the system after nanoparticle injection, and the damaged system for the experiments conducted with alumina nanoparticles of 90 nm diameter suspended aqueous solution in an oil sands packed bed column with clean silica sand of 30−40 mesh size saturated with La Hocha crude oil. Other experimental conditions include residence time, 24 h; porosity, 33%; pressure, 6.9 MPa; and temperature, 323 K.

of saturation, in the presence of nanoparticles, the relative permeability of the crude oil (Kro) was significantly higher than the relative permeability of the base curve (Kro,b). In addition, after the use of nanoparticles, the damage was induced upon the third step, which indicates that the Kro was higher than the Kro,b for water saturation (Sw) values in the range of 0.3 to 0.7. These results show that the nanoparticles can significantly inhibit the damage associated with asphaltenes deposition. Additionally, the final induced damage (in the third step) demonstrates that the nanoparticle treatment was effective and preserved the perdurability of the system. However, the Swr had an initial value of 7%, and after the injection of nanoparticles, the Swr increased to 23%. This phenomenon was likely due either to nanoparticle deposition onto the surface rock, which created a monolayer, or to the stabilizing effect of nanoparticles in the porous media, which stabilized the asphaltenes in the crude oil by the interaction of intermolecular forces. The latter phenomenon could control the water production in hydrocarbon reservoirs in a similar manner as conventional relative permeability reducers (RPM). Following the induction of damage, the Swr changed to 5%, which indicates that the nanoparticles were able to inhibit the damage because of the preference of asphaltenes to be captured by the nanoparticles. With respect to the residual saturation of crude oil (Sor), the initial value was approximately 25% and demonstrated four points of reduction following the nanoparticle injection, which indicates a possibility for increasing the recovery.

The recovery curves are shown in Figure 5. As seen, the recovery increases with the treatment injection. Initially (<2

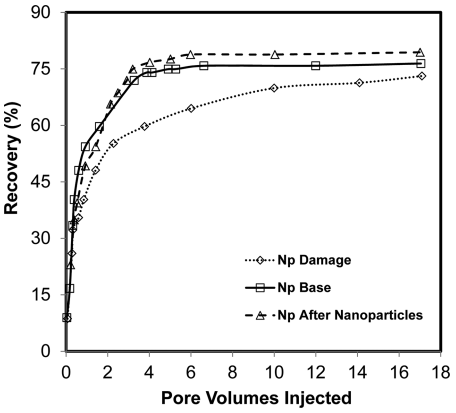

Figure 5. Recovery curves for (1) the base system; (2) the system after nanoparticle injection (where 0.5 PV of nanofluids was injected simultaneously with crude oil, followed by injection of 0.5 PV of *n*-heptane); and (3) the damaged system (where 0.5 PV of *n*-heptane was injected without the presence of nanoparticles to generate damage). Other experimental conditions include porosity, 33%; pressure, 6.9 MPa;, and temperature, 323 K.

PV), after nanoparticle injection was measured and the recovery curve was analyzed. The asphaltenes deposited on the rock surface suggest that the porous media could be less water wettable than in the washed sand pack case. After 2 PV, the oil production could drag the deposited reaching critical velocity. Then, the system becomes more water wettable as expected by the use of the nanoparticles, which, in fact, modify the wettability of rock surface. These phenomena could be evidenced in the Swr and Sor. Finally, the recovery increases from 73% in the damaged system to 80% after the nanoparticle injection, which indicates that the nanoparticles are able to restore production, yielding an improvement in the recovery due to the ability of the nanoparticles to adsorb and stabilize the asphaltenes content of the system.

4. CONCLUSIONS

Asphaltenes adsorption isotherms of twelve nanoparticles and reservoir rocks were determined. The adsorption isotherms were fit to the Freundlich and Langmuir models. With respect

dx.doi.org/10.1021/ef4000825 | *Energy Fuels* XXXX, XXX, XXX−XXX

to the SHS samples, the experimental data in the asphaltene sorption isotherms were adequately modeled by the Freundlich model. However, for the silica gel (amorphous), the silica gel (commercial), AlNi15, and PdNi/Al, the Langmuir was the best fit, which demonstrated a Type I isotherm (a monolayer). The asphaltene uptake (Figure 2) decreased in the order of AlNi15 > SNi15 > SNi5 > AlNi5 ≈ silica gel (amorphous) > silica gel (crystalline) > AlII > fumed silica gel > zeolite > PdNi/Al >AlI > washed rock ≈ unwashed rock > silica gel (commercial). Complete asphaltene sorption on alumina-SHS was achieved rapidly, which makes this material a candidate for inhibiting the precipitation and deposition of asphaltenes on rock surfaces.

Only the nanoparticles that adsorb strongly the more polar compounds are capable of neutralizing the polar forces that remain active during weak adsorption to cause multilayer adsorption. That inhibition prevents both flocculation and precipitation, which these polar compounds seem to be the building blocks of, and eliminates their tendency to adsorb in multilayers, which could be due to remaining polarity of the initially adsorbed asphaltenes.

The injection of nanofluids into porous media showed an inhibition in the agglomeration, precipitation, and deposition of asphaltenes on the rock surfaces, which was based on a three-step displacement test. Additionally, the nanoparticle treatment demonstrated an enhanced perdurability of the system. The nanoparticles were able to restore production and led to improvements in recovery due to their ability to adsorb and stabilize the asphaltenes content of the system.

■ AUTHOR INFORMATION

Corresponding Author

*E-mail: fbcortes@unal.edu.co.

Notes

The authors declare no competing financial interest.

■ ACKNOWLEDGMENTS

The authors acknowledge Prof. Dr. Sergio Lopera for fruitful discussions and assistance. The authors are grateful to Petroraza SAS, COLCIENCIAS, and Universidad Nacional de Colombia for logistical and financial support.

■ REFERENCES

(1) Joshi, N. B.; Mullins, O. C.; Jamaluddin, A.; Creek, J.; McFadden, J. Asphaltene precipitation from live crude oil. *Energy Fuels* **2001**, *15*, 979−86.

(2) Bouhadda, Y.; Bormann, D.; Sheu, E.; Bendedouch, D.; Krallafa, A.; Daaou, M. Characterization of Algerian Hassi-Messaoud asphaltene structure using Raman spectrometry and X-ray diffraction. *Fuel* **2007**, *86*, 1855−1864.

(3) Yen, T. F., Chilingarian, G. V. *Asphaltenes and Asphalts, Developments in Petroleum Science*; Elsvier: Amsterdam, 1994.

(4) Groenzin, H.; Mullins, O. C. Asphaltene molecular size and structure. *J. Phys. Chem. A* **1999**, *103*, 11237−45.

(5) Pedersen, K. S.; Christensen, P. L. *Phase Behavior of Petroleum Reservoir Fluids*, 1st ed.; Taylor & Francis Group: Boca Ratón, FL, 2007.

(6) Leontaritis, K. J.; Amaefule, J. O.; Charles, R. E. A systematic approach for the prevention and treatment of formation damaged caused by asphaltene deposition. *SPE Prod. Facil.* **1994**, *64*, 8−157.

(7) Yan, J.; Plancher, H.; Morrow, N. R. Wettability changes induced by adsorption of asphaltenes. *Soc. Pet. Eng. J.* **1997**, *12* (4), 259−266.

(8) Acevedo, S.; Ranaudo, M. A.; Escobar, G.; Gutierrez, L.; Ortega, P. Adsorption of asphaltenes and resins on organic and inorganic substrates and their correlation with precipitation problems in production well tubing. *Fuel* **1995**, *74*, 595−598.

(9) Rudrake, A.; Karan, K.; Horton, J. A combined QCM and XPS investigation of asphaltene adsorption on metal surfaces. *J. Colloid Interface Sci.* **2009**, *332*, 22−31.

(10) Abdallah, W.; Taylor, S. Surface characterization of adsorbed asphaltene on a stainless steel surface. *Nucl. Instrum. Methods Phys. Res., Sect. B.* **2007**, *258*, 213−217.

(11) Xie, K.; Karan, K. Kinetics and thermodynamics of asphaltene adsorption on metal surfaces: A preliminary study. *Energy Fuels* **2005**, *19*, 1252−1260.

(12) Mendoza, J.; Castellanos, I.; Ortiz, A.; Buenrostro, E.; Durán, C.; López, S. Study of monolayer to multilayer adsorption of asphaltenes on reservoir rock minerals. *Colloids Surf., A* **2009**, *340*, 149−154.

(13) Kumar, K.; Dao, E.; Mohanty, K. J. AFM study of mineral wettability with reservoir oils. *J. Colloid Interface Sci.* **2005**, *289*, 206−217.

(14) Drummond, C.; Israelachvili, J. Fundamental studies of crude oil−surface water interactions and its relationship to reservoir wettability. *J. Pet. Sci. Eng.* **2004**, *45*, 61−81.

(15) Gonzalez, G.; Moreira, M. B. C. The wettability of mineral surfaces containing adsorbed asphaltenes. *Colloids Surf.* **1991**, *58*, 293−302.

(16) Pernyeszi, T.; Dékány, I. Asphaltene adsorption on clays and crude oil reservoir rocks. *Colloids Surf., A* **1998**, *137*, 373−384.

(17) Saada, A.; Siffert, B.; Papirer, E. Comparison of the hydrophilicity/ hydrophobicity of illites and kaolinites. *J. Colloid Interface Sci.* **1995**, *174*, 185−190.

(18) Marlow, B. J.; Sresty, G. C.; Hughes, R. D.; Mahajan, O. P. Colloidal stabilization of clays by asphaltenes in hydrocarbon media. *Colloids Surf.* **1987**, *24*, 283−297.

(19) Dubey, S. T.; Waxman, M. H. Asphaltene adsorption and desorption from mineral surfaces. *SPE Reservoir Eng.* **1995**, *6* (3), 389−395.

(20) Piro, G.; Canonico, L. B.; Galbariggi, G.; Bertero, L.; Carniani, C. Asphaltene adsorption onto formation rock: an approach to asphaltene formation damage prevention. *SPE Prod. Facil.* **1995**, *11* (3), 156−160.

(21) Acevedo, S.; Ranaudo, M.; García, C.; Castillo, J.; Fernández, A.; Caetano, M.; Goncalvez, S. Importance of asphaltene aggregation in solution in determining the adsorption of this sample on mineral surfaces. *Colloids Surf., A* **2000**, *166*, 145−142.

(22) Sakanishi, K.; Saito, I.; Watanabe, I.; Mochida, I. Dissolution and demetallation treatment of asphaltene in resid using adsorbent and oil-soluble Mo complex. *Fuel* **2004**, *83*, 1889−1893.

(23) Acevedo, S.; Castillo, J.; Fernandez, A.; Goncalves, S.; Ranaudo, M. Study of multilayer adsorption of asphaltenes on glass surface by photothermal surface deformation. Relation of this adsorption to aggregate formation in solution. *Energy Fuels* **1998**, *12*, 386−390.

(24) Marczewski, A. W.; Szymula, M. Adsorption of asphaltene from toluene on mineral surface. *Colloids Surf., A* **2002**, *208* (1−3), 259−266.

(25) Szymula, M.; Marczewski, A. W. Adsorption of asphaltenes from toluene on typical soils of Lublin Region. *Appl. Surf. Sci.* **2002**, *196* (1−4), 301−311.

(26) Marczewski, A. W.; Szymula, M. Adsorption of asphaltenes from toluene on quartz and silica-rich soils. *Ann. UMCS* **2003**, *LVIII*, 69−79.

(27) Mohammadi, M.; Akbari, M.; Fakhroueian, Z.; Bahramian, A.; Azin, R.; Arya, S. Inhibition of asphaltene precipitation by TiO_2, SiO_2, and ZrO_2 nanofluids. *Energy Fuels* **2011**, *25* (7), 3150−3156.

(28) Karimi, A.; Fakhroueian, Z.; Bahramian, A.; Khiabani, N. P.; Darabad, J. B.; Azin, R.; Arya, S. Wettability alteration in carbonates using zirconium oxide nanofluids: EOR implications. *Energy Fuels* **2012**, *26* (2), 1028−1036.

(29) Ayatollahi, S.; Zerafat, M. M.Nanotechnology-assisted EOR techniques: New solutions to old challenges. *SPE Int. Oilfield Nanotechnol. Conf.* **2012**, http://dx.doi.org/10.2118/157094-MS.

(30) Nassar, N. N. Asphaltene adsorption onto alumina nanoparticles: Kinetics and thermodynamic studies. *Energy Fuels* **2010**, *24*, 4116−4122.
(31) Hashemi, R.; Nassar, N. N.; Pereira-Almao, P. Transport behavior of multimetallic ultradispersed nanoparticles in an oil-sands-packed bed column at a high temperature and pressure. *Energy Fuels* **2012**, *26* (3), 1645−1655.
(32) Nassar, N. N.; Hassan, A.; Pereira-Almao, P. Comparative oxidation of adsorbed asphaltenes onto transition metal oxide nanoparticles. *Colloids Surf., A* **2011**, *384* (1−3), 145−149.
(33) Nassar, N. N.; Hassan, A.; Pereira-Almao, P. Metal oxide nanoparticles for asphaltene adsorption and oxidation. *Energy Fuels* **2011**, *25* (3), 1017−1023.
(34) Nassar, N. N.; Hassan, A.; Pereira-Almao, P. Thermogravimetric studies on catalytic effect of metal oxide nanoparticles on asphaltene pyrolysis under inert conditions. *J. Therm. Anal. Calorim.* **2011**, *110* (3), 1327−1332.
(35) Maghzi, A.; Mohebbi, A.; Kharrat, R. Pore-scale monitoring of wettability alteration by silica nanoparticles during polymer flooding to heavy oil in a five-spot glass micromodel. *Transp. Porous Media* **2011**, *3*, 653−664.
(36) Ju, B.; Dai, S.; Luan, Z.; Zhu, T.; Su, X.; Qiu, X. Study of wettability and permeability change caused by adsorption of nanometer structured polysilicon on the surface of porous media. *SPE* **2002**; http://dx.doi.org/10.2118/77938-MS.
(37) Ju, B. S.; Fan, T.; Ma, M. Enhanced oil recovery by flooding with hydrophilic nanoparticles. *China Particuol.* **2006**, *4*, 41−46.
(38) Onyekonwu, M.; Ogolo, N. A. Investigating the use of nanoparticles in enhancing oil recovery. *SPE* **2010**, http://dx.doi.org/10.2118/140744-MS.
(39) Cortés, F. B.; Mejía, J. M.; Ruiz, M. A.; Benjumea, P.; Riffel, D. B. Sorption of asphaltenes onto nanoparticles of nickel oxide supported on nanoparticulated silica gel. *Energy Fuels* **2012**, *26*, 1725−1730.
(40) Franco, C.; Patiño, E.; Benjumea, P.; Ruiz, M. A.; Cortés, F. B. Kinetic and thermodynamic equilibrium of asphaltenes sorption onto nanoparticles of nickel oxide supported on nanoparticulated alumina. *Fuel* **2012**, http://dx.doi.org/10.1016/j.fuel.2012.06.022.
(41) Nogami, M.; Moriya, Y. J. Glass formation through hydrolysis of $Si(OC_2H_5)_4$ with NH_4OH and HCl Solution. *J. Non-Cryst. Solids* **1980**, *37*, 191−201.
(42) Brinker, C. J.; Keefer, K. D.; Schaefer, D. W.; Assink, R. A.; Kay, B. D.; Ashley, C. S. Sol−gel transition in simple silicates II. *J. Non-Cryst. Solids* **1984**, *63*, 45−59.
(43) Cortes, F. B.; Chejne, F.; Carrasco-Marín, F.; Pérez-Cadenas, A.; Moreno-Castilla, C. Water sorption on silica- and zeolite-supported hygroscopic salts for cooling system applications. *Energy Convers. Manage.* **2012**, *53*, 219−223.
(44) Rouquerol, F; Rouquerol, J; Sing, K. S. W. Adsorption by powders and porous solids: Principles, methodology, and applications. Academic Press: London; 1999.
(45) Brunauer, S.; Emmett, P. H.; Teller, E. Adsorption of gases in multi-molecular layers. *J. Am. Chem. Soc.* **1938**, *60*, 309−19.
(46) Langmuir, I. The constitution and fundamental properties of solids and liquids. Part I: Solids. *J. Am. Chem. Soc.* **1916**, *38* (11), 2221−2295.
(47) Freundlich, H. M. F. Uber die adsorption in losungen. *Z. Phys. Chem. (Leipzig)* **1906**, *57(A)*, 385−470.
(48) Dudášová, D.; Simon, S.; Hemmingsen, P.; Sjöblom, J. Study of asphaltenes adsorption onto different minerals and clays. Part 1. Experimental adsorption with UV depletion detection. *Colloids Surf., A* **2008**, *317*, 1−9.
(49) Riffel, D. B.; Schmidt, F. P.; Belo, F. A.; Leite, A. P. F.; Cortés, F. B.; Chejne, F.; Ziegler, F. Adsorption of water on Grace Silica Gel 127B at low and high pressure. *Adsorption* **2011**, *17*, 977−984.
(50) Nassar, N. N.; Hassan, A.; Pereira-Almao, P. Effect of the particle size on asphaltene adsorption and catalytic oxidation onto alumina particles. *Energy Fuels* **2011**, *25* (9), 3961−3965.
(51) Nassar, N. N.; Hassan, A.; Pereira-Almao, P. Effect of surface acidity and basicity of aluminas on asphaltene adsorption and oxidation. *J. Colloid Interface Sci.* **2011**, *360*, 233−238.